Mapping the optical properties of slab-type two-dimensional photonic crystal waveguides

Eric Dulkeith,* Sharee J. McNab, and Yurii A. Vlasov
IBM T. J. Watson Research Center, Yorktown Heights, New York 10598, USA
(Received 19 April 2005; published 1 September 2005)

We report on systematic experimental mapping of the transmission properties of two-dimensional silicon-on-insulator photonic crystal waveguides for a broad range of hole radii, slab thicknesses, and waveguide lengths for both TE and TM polarizations. Detailed analysis of numerous spectral features allows a direct comparison of experimental data with three-dimensional plane-wave and finite-difference time-domain calculations. We find that the bandwidth for low-loss propagation completely vanishes for structural parameters where the photonic band gap is maximized. Our results demonstrate that in order to maximize the bandwidth of low-loss waveguiding the hole radius must be significantly reduced. While the photonic band gap considerably narrows, the bandwidth of low-loss propagation in PhC waveguides is increased up to 125 nm with losses as low as 8 ± 2 dB/cm.

DOI: 10.1103/PhysRevB.72.115102 PACS number(s): 78.20.Ci, 42.70.Qs, 41.20.Jb

I. INTRODUCTION

Over the past years interest in two-dimensional photonic crystals (PhC's) has intensified and is regarded these days as a promising platform for dense integration of planar photonic integrated circuits on a chip-scale level.[1–19] In particular, PhC's waveguides fabricated on silicon-on-insulator (SOI) provide waveguide cross-sectional areas on the submicron scale level while maintaining single-mode operation due to high refractive index contrast.[4–14] It has been shown that for triangular lattice membrane-type PhC's,[15–17] consisting of a periodic array of holes with a silicon slab thickness h around $0.5a$ and hole radii of $\sim 0.35a$ (a is the lattice constant), the bandwidth of the photonic band gap (PBG) can extend over most of the 1.3- and 1.5-μm telecommunications transmission bands. Single-mode waveguiding can be realized by removing a single row of holes in the periodic photonic lattice along the Γ-K direction.[16,17] Mode confinement in the vertical direction is accomplished by index guiding, while lateral confinement within the silicon slab plane is defined by the PBG.[18] This hybrid confinement limits the bandwidth for intrinsically lossless propagation to frequencies that are below the light line cutoff. Thence propagation becomes lossy with mode leakage out of the slab.[6,10] Consequently, the bandwidth for intrinsically low-loss propagation (LLP) of the waveguiding mode is restricted to only a fraction of the PBG, e.g., in the order of only a few tens of nanometers.[7–10,13,14] These insights and other theoretical investigations of light confinement in planar PhC's and PhC waveguides have been examined in detail and are well understood. In contrast, experimental studies of the waveguiding properties of slab-type PhC waveguides have been hindered for a long time by difficulties in fabricating these structures. One of the major challenges in the last decade was to overcome extremely high transmission losses due to surface roughness, structural irregularities, and inefficient coupling, which significantly complicated the interpretation of experimental results. Recent achievements in optimizing the light coupling efficiency into the PhC as well as fabrication improvements that reduce surface roughness have led to ultra-low-loss PhC waveguides, thus enabling further spectroscopic exploration.[10,11,13,14]

In this paper, we present detailed and comprehensive experimental studies of the transmission properties of TE-like (even parity with respect to the slab plane) and TM-like (odd parity with respect to the slab plane) modes of two-dimensional membrane-type PhC waveguides. The spectral properties are measured as a function of various lattice parameters such as hole radius r, slab thickness h, and the crystal length l. We focus predominantly on the impact of structural parameters on the LLP bandwidth. A survey of the applied experimental techniques, fabrications methods, and theoretical calculations is given in Sec. II. In Sec. III we explore the transmission properties of the PhC waveguides with structural parameters optimized for a maximum band gap. We show that for large hole radii of $r/a \sim 0.38$ the bandwidth for LLP completely disappears due to effective interaction with the band edge slab modes of the PhC. The transmission properties of PhC waveguides with small hole radii spanning from $r/a=0.22$ to 0.34 are investigated in Sec. IV. The results exhibit that in order to maximize the bandwidth of the waveguiding mode the hole radius needs to be reduced to $r/a \sim 0.2$. Although this optimization is accompanied by a significant decrease of the PBG, the bandwidth for propagation is increased up to 125 nm, maintaining a reasonable trade-off between band gap and propagation bandwidth. The experimental findings are compared to three-dimensional (3D) plane-wave calculations using the MIT photonic band code[19] and 3D finite-difference time domain (FDTD).[20] For the propagation bandwidth-optimized parameters, we determine losses as small as 8 ± 2 dB/cm, which is one of the lowest reported to date. Section V examines the experimental transmission spectra for TM-polarized light. After their comparison with photonic band structures, in Sec. VI we address the observed coupling of even TE- with odd TE- and TM-like modes. Results are summarized in Sec. VII.

II. EXPERIMENT

Devices are fabricated on lightly p-doped 200-mm SOI wafers from SOITEC (Ref. 24) with a Si device layer thickness h of 220 nm on top of a 2-μm buried oxide layer

(BOX). The processing is performed on a standard CMOS fab line at the IBM Watson Research Center as described elsewhere.[10,11] A 50-nm-thick oxide is deposited via chemical vapor deposition to serve as a hard mask for etching. The wafers are patterned by electron beam lithography (LEICA-VB6, 100 keV, single writing field 400 μm). The oxide hard mask is opened and the silicon device layer is dry-etched $CF_4/CHF_3/Ar$ and HBr chemistry, respectively. After structure definition, the BOX layer is selectively underetched in a buffered HF to form suspended membranes. The PhC waveguides are defined by omitting one row of holes from the PhC lattice in the Γ-K direction (W1-type waveguide). Light is coupled to the PhC waveguide via butt-coupled single-mode strip waveguides. Once the PhC membrane is defined, polymer-inverted spot-size converters are fabricated to achieve high coupling efficiency as reported elsewhere.[10,11] Three different wafers with slightly different slab thicknesses h were processed with PhC waveguides having nominally the same lattice constant $a=437.5$ nm, but different hole radii $r=96$, 140, and 165 nm ($r/a=0.22$, 0.32, and 0.35, respectively). The PhC waveguide length was varied in each writing field from 29 to 2000 μm for accurate loss determination. Four of such fields grouped together constitute one experimental chip with the e-beam exposure dose intentionally varied between each field. This allows the phase space of explored lattice parameters to be further broadened. In addition, proximity effects due to background electron beam scattering induce minor changes in the hole diameter between the different PhC waveguides even within one field. Such variation allows the exploration of a quasi-continuous range of different lattice parameters, but at the same time requires thorough statistical analysis of the particular PhC waveguide on a given chip.

The lattice constant a, Si slab thickness h, and the hole radius r of a given sample are determined by statistical evaluation of scanning tunneling microscope (SEM) images obtained on a LEO SEM1560 model with identical imaging conditions (acceleration voltage, focal distance, magnification, column and aperture alignment, etc.). Over 110 PhC waveguides are characterized in total. The lattice constant was measured four times for each PhC waveguide (total number of measurements $N=440$), yielding an overall value of $a=437.6$ nm with a standard deviation of only $\sigma=0.93$ nm.

In order to check the variation of the hole radius along a single PhC waveguide $N=60$ holes were measured at three different locations along the longest 2000-μm-long waveguide (separation approximately 600 μm). The results yield statistically identical mean hole radii of 99.21 nm at one end of the PhC waveguide, 99.18 nm in the middle section, and 98.17 nm at the other end with standard deviations not exceeding 1.2 nm. The overall mean hole radius for the total of $N=180$ measurements was found to be 98.9 nm with $\sigma=1.12$ nm. For all other PhC waveguides the hole radius was measured only six times in their middle section. Although this small number imposes a less accurate estimation of the mean value, however, from the $N=180$ measurements the resulting standard error does not exceed 0.5% for $N=6$. The slab thickness h of the wafers was measured at nine different positions along each sample. For the three processed SOI wafers with devices having $r/a=0.22$, 0.32, and 0.35 the normalized thickness of the Si slab was measured to be $h/a=0.518$, 0.507, and 0.546, respectively.

Measurements of transmission spectra of PhC waveguides are performed using a broadband (1200–1700 nm) LED source and an optical spectrum analyzer (OSA) with 5 nm spectral resolution. A rejection ratio of over 30 dB between TE and TM polarizations is achieved with the use of polarization maintaining, tapered and lensed fibers, and a polarization controller. The transmission spectra of the PhC waveguides are normalized to the transmission spectra of corresponding single-mode reference strip waveguides located in the same writing field near the PhC structures as described elsewhere.[10,11]

The experimental results are compared with 3D plane-wave calculations performed using the MIT photonic-band code.[19] The dielectric permittivity ε_{Si} of the Si slab and ε_{SiO_2} of the oxide layer are taken as 12.1 and 2.0, respectively. Values for the hole radii and lattice constant are chosen as determined by SEM measurements. The grid resolution (number of vectors in the unit cell of the PhC) of the plane-wave calculations is set to $16\times16\times16$ to achieve a reasonable trade-off between the error in eigenvalue convergence (below $\sim$2% and calculation time.[19] However, the limited resolution imposes a drawback that very small changes in the slab thickness h are not well resolved. This results in a weak steplike rather than a smooth dependence of the calculated band structures on h. To overcome this issue, the photonic crystal band structures for slab thicknesses with $h/a=0.4$, 0.5, 0.6, and 0.7 are calculated and intermediate values are interpolated. Interestingly, to achieve the best agreement between experiment and theory all slab thicknesses needed to be assumed 5%–10% thinner than measured by SEM. This discrepancy is consistent with a small, but noticeable thinning of the silicon slab in the membrane region during the BOX etching.

All calculations of transmission spectra are performed with a 3D FDTD method using the FULLWAVE software package.[20] Transmission through a 33-unit-cell-long PhC W1 waveguide with 13 rows of holes on each side is calculated with a $265\times243\times551$ mesh (20 nm grid size) for over 250 000 time steps.

III. PHC WAVEGUIDES WITH MAXIMIZED PHOTONIC BAND GAP (TE-LIKE MODES)

Historically most efforts on both three-dimensional and two-dimensional PhC's were focused on maximizing the bandwidth of the PBG.[15] A large variety of different hole shapes and crystal symmetries were explored in a planar 2D geometry. It was shown[15] that for 2D PhC's a triangular lattice of air holes (hexagonal first Brillouin zone) produces the widest PBG for a slab thickness of $\sim0.5a$ and hole radii of $\sim0.35a$. It is known, however, that a guided mode caused by a defect line in the PhC suffers severely from out-of-plane light leakage for frequencies above the light line. Leakage losses were measured[6,10] to be as high as 1500 dB/cm, which prohibits the utilization of this wavelength range for useful waveguiding. These inevitable diffraction losses limit

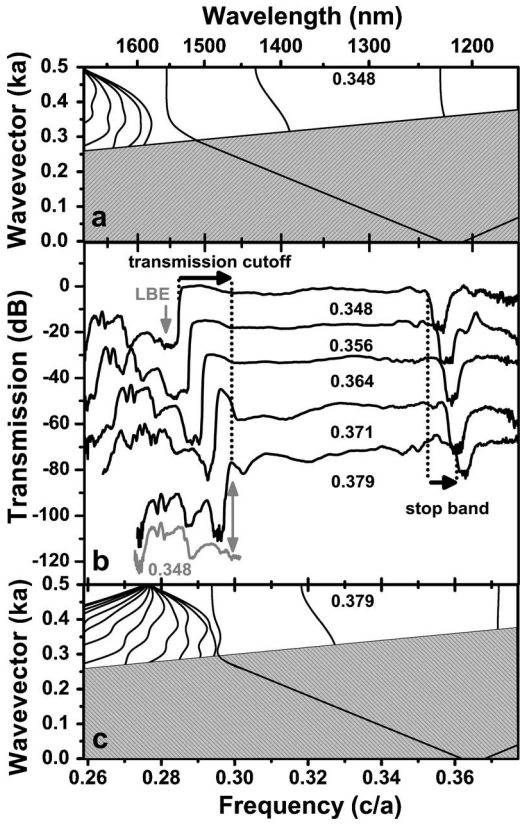

FIG. 1. Comparison of experimental TE transmission spectra of PhC waveguides with large hole radii against 3D plane-wave band structure calculations. (a) Band structure for a PhC waveguide with $r/a=0.348$. (b) Set of transmission spectra for PhC waveguides, equal in length ($l=29$ μm) but with increasing hole radius $r/a=0.348-0.379$. The grey curve illustrates the spectral merge of lower photonic band edge (LBE) and waveguiding onset for the PhC with $r/a=0.379$ (slab modes for $r/a=0.348$ shifted with respect to the normalized frequency for comparison with the modes for $r/a=0.379$). (c) Band structure for a PhC waveguide with a hole radius of $r/a=0.379$.

the bandwidth for intrinsic LLP below the light line to only a fraction of the PBG.[7–10,13,14] In this section we will present the transmission properties of triangular 2D PhC waveguides as a function of the hole radius that are chosen to match the conditions for an optimized PBG ($r/a=0.348-0.384$).

Figure 1 shows a series of transmission spectra of PhC waveguides of identical length (29 μm), but different hole radii, and compares them with photonic band structure calculations. A number of spectral features of the TE-like modes can be directly mapped to the band diagram. Figure 1(a) presents the photonic band structure for the PhC waveguide with the smallest radius of $r/a=0.348$. The onset of the waveguiding mode at wavelengths around 1550 nm, also known as the mode gap cutoff,[7,8] is clearly seen. In the corresponding measured spectrum, this onset results in a sharp transmission cutoff around 1535 nm [Fig. 1(b), upper curve]. The bandwidth for intrinsic LLP is strictly bounded by this and the crossing of the waveguide mode with the light line. Calculations show that the light line cutoff is at $\sim$1510 nm (normalized frequency of $0.29c/a$). Since the length of the PhC waveguide is only 60 unit cells, the light line cutoff manifests itself only as a weak kink at $\sim$1505 nm in the experimental spectra. The LLP bandwidth is determined to be $\sim$30 nm. At longer wavelengths, small resonances are present in the measured transmission spectrum. According to the photonic band structure, these resonances are identified as a series of slab modes below the lower photonic band edge (LBE). These modes are delocalized over the whole slab with their fields mainly concentrated in the dielectric material (dielectric bands).[15,16] At shorter wavelengths, around 1230 nm, the transmission reveals a distinct stop band. This stop band opens due to the folding of the waveguiding mode at the edge of the Brillouin zone at $k=0$. The upper band edge (UBE), which is defined by the commencement of slab modes that are predominately located in the holes (air bands),[15,16] is not observed in the current set of spectra since it lies at 1110 nm ($0.40c/a$), as determined by band structure calculations.

The series of transmission spectra in Fig. 1(b) shows that as the hole radius increases, all characteristic spectral features of the PhC waveguide undergo a shift to higher energies. This is confirmed by the photonic band structure in Fig. 1(c) ($r/a=0.379$). This behavior is easily explained by a decrease of the effective refractive index of the slab. However, in addition, the spectral shape of the transmission in the region of LLP changes drastically. For the smallest hole radius the LLP transmission region is characterized with a nearly flat top profile. Propagation losses for waveguides with holes of approximately the same radius were measured previously to be as small as 24 ± 3 dB/cm. In contrast, for PhC waveguides with larger hole radii, first, the flat top profile of the LLP gradually narrows and then completely disappears for $r/a=0.379$. Second, propagation losses in this region increase to 70 dB/cm, indicating the complete vanishing of the LLP for PhC waveguides with large holes.

Analyzing Fig. 1, it can be seen that with increasing hole radius the blueshift of the transmission cutoff is far more pronounced than the corresponding blueshift of the stop band. This is surprising since both stem from the same waveguiding mode. To clarify this issue the experimental results over a large number of PhC waveguides with different hole radii are summarized in Fig. 2. The spectral positions of waveguiding mode onset, stop band, light line cutoff, and onset of the LBE slab modes are plotted against the normalized hole radius. Since both the mode onset and the stop band are defined by the same PhC waveguiding mode, a change in radius should lead to a parallel wavelength shift. The experimental results for $r/a<0.37$ confirm this behavior. Consequently, the bandwidth for LLP continuously shrinks with increasing the hole radius. The experimental results show that the LBE exhibits a stronger dependence on the hole radius than the waveguiding mode. This is due to the fact that these dielectric modes are delocalized over the whole slab region and are thus strongly affected by even small changes in the hole radius. Contrary to this, the field energy of the PhC waveguiding mode is almost completely confined in the hole-free defect line of the photonic crystal and hence the spectral position of the waveguiding mode is less influenced by the holes in the slab. As a result, for hole radii with $r/a>0.37$ the experimental transmission cutoff is

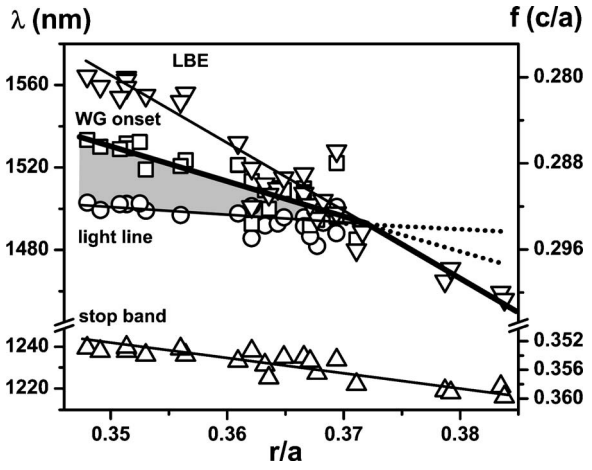

FIG. 2. Experimentally determined TE map of spectral positions of lower band edge (LBE), waveguiding onset, light line, and stop band as a function of the normalized hole radius for $r/a=0.348-0.384$. The grey shaded area shows the frequency region for low-loss propagation (lines are guides for the eye).

no longer defined by the waveguiding mode onset, but rather by the onset of the slab modes at the LBE. This causes the LLP bandwidth to completely vanish for large hole radii.

This experimental observation is confirmed by photonic band structure calculations shown in Figs. 1(a) and 1(c). While for $r/a=0.348$ the waveguiding onset and the LBE are clearly spectrally separated, for $r/a=0.379$ the LBE overlaps with the waveguiding mode. Thus, light from the access strip waveguide can couple not only effectively to the PhC waveguiding mode, but also to the slab modes and hence leaks into the slab. This explains the dramatic increase of the propagation losses. For PhC waveguides with $r/a>0.37$, it leads to zero bandwidth for low-loss propagation. The results presented in this section demonstrate that with structural parameters, chosen to maximize the PBG, the bandwidth for LLP finally vanishes.

IV. PHC WAVEGUIDES WITH MAXIMIZED LOW-LOSS PROPAGATION BAND (TE-LIKE MODES)

Instead of optimizing the bandwidth of the PBG (a parameter rather irrelevant for the implementation of PhC waveguides in integrated optics), it is more meaningful to optimize the bandwidth of LLP. From the analysis of the previous results we can conclude that smaller hole radii are required for the optimization of the LLP bandwidth. In Fig. 2 we have seen that for a decrease of the hole radius of only $\sim 5\%$ $(r/a=0.365\rightarrow 0.348)$ the LLP bandwidth significantly broadens by more than a factor of 2 $(13\rightarrow 30$ nm). To confirm this trend this section will first deal with PhC waveguides of only slightly smaller hole radii $(r/a=0.32-0.34)$. In the second part we will then proceed to investigate PhC waveguides with very small holes $(r/a=0.22-0.24)$.

The experimental transmission spectra of PhC waveguides with different lengths from 29 to 2000 μm but approximately the same hole radius $(r/a\sim 0.34)$ are shown

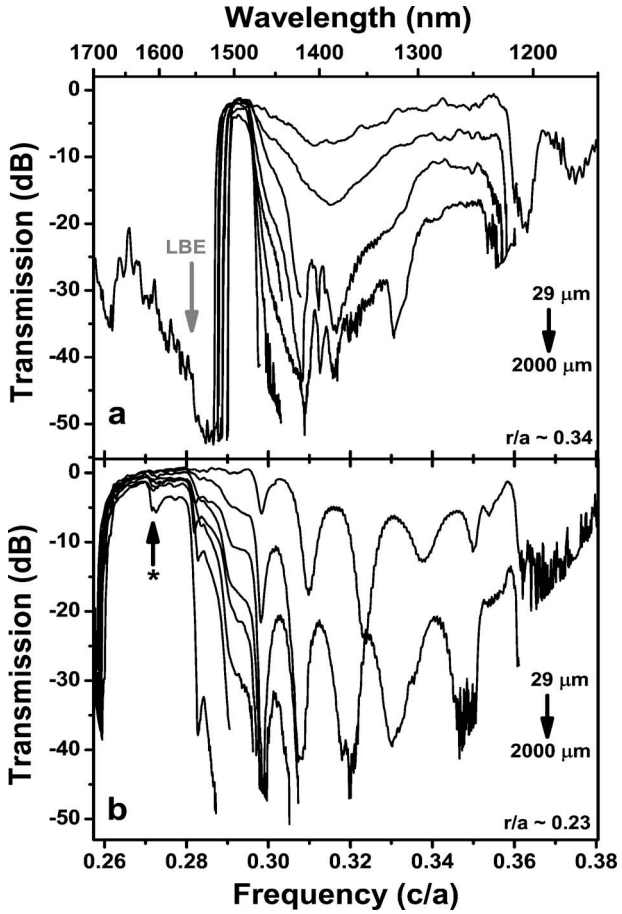

FIG. 3. Length series of TE transmission spectra of PhC waveguides (29–2000 μm) for two different hole radii: (a) $r/a\sim 0.34$ and (b) $r/a\sim 0.23$. The transmission dip marked with an asterisk corresponds to the x-odd TE-like mode (see text for details).

in Fig. 3(a). In the same manner as done in Fig. 1, the comparison of transmission spectra with photonic band structure calculations (not shown) enables the identification of the spectral features of the PhC waveguides. For a waveguide length of 29 μm (upper curve), the LBE is clearly visible in the long-wavelength region at 1560 nm. The sharp transmission cutoff, located at 1515 nm, corresponds to the waveguiding onset. The light line cutoff is seen at 1480 nm. At shorter wavelengths, the transmission spectrum displays a stop band at 1220 nm. In fact, the spectra look very similar to the results of Fig. 1(b); however, the PBG bandwidth is significantly reduced by 25 nm, while the bandwidth for LLP increases up to 35 nm. The results of Fig. 3(a) can be used to determine the propagation losses in the LLP region. Losses at 1500 nm are determined to be 20 ± 3 dB/cm; the method is described later in this section (see also Ref. 10).

Since the expansion of the bandwidth for LLP simultaneously takes place with a shrinking of the PBG, one can conclude that there must be a lower limit for the radius where the LLP bandwidth would be restricted by the slab modes of the UBE. To find the upper limit of the LLP bandwidth, PhC waveguides with significantly reduced hole radii need to be investigated. Figure 3(b) shows the experimental

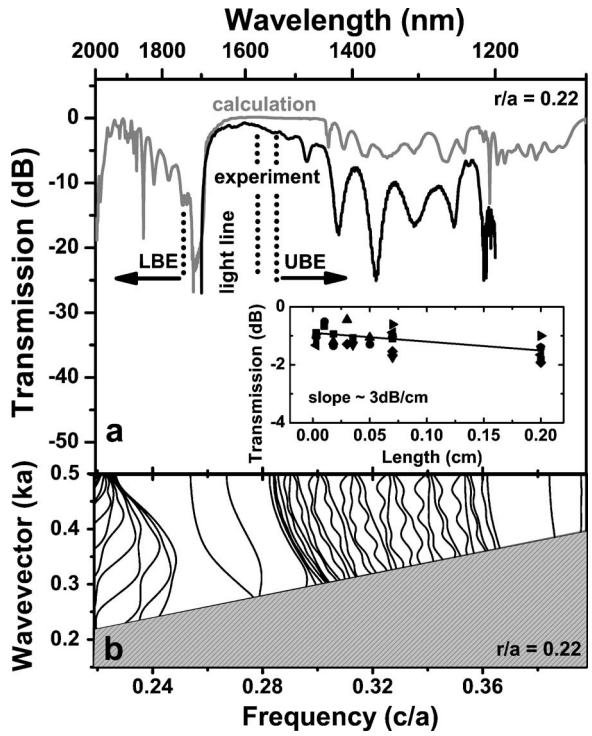

FIG. 4. (a) Experimental TE transmission spectra (black line) of a 29-μm PhC waveguide with $r/a=0.22$ compared with 3D FDTD calculations (grey line). Inset: normalized transmission at 1650 nm of PhC waveguides as a function of the length. From the slope, the losses of the whole photonic circuit (PhC and strip waveguides) are determined as 3 ± 2 dB/cm. This corresponds to 8 ± 2 dB/cm loss for the PhC waveguide (see text for details). (b) 3D plane-wave band structure calculations with the same structural input parameters as for the FDTD calculations in (a).

results of a series of transmission spectra of PhC waveguides with different lengths and again with nearly the same hole radii ($r/a\sim0.23$). Compared to Fig. 3(a), the radius is reduced by over 30% and causes a drastic change in the transmission spectra. Within the measured spectral range, no LBE is detected, since it is redshifted to 1730 nm. Furthermore, the stop band has also disappeared from the spectra. On the very edge of the transmission spectra, around 1695 nm, a sharp transmission cutoff is present followed by a region of flat transmission with relatively low losses. For wavelengths shorter than 1550 nm, the spectra are now dominated by very strong resonances covering a broad bandwidth.

To understand the origin of these resonances and to interpret the experimental transmission spectra, Fig. 4(a) compares the transmission spectrum of a 29-μm PhC waveguide with $r/a=0.22$ against 3D FDTD calculations. The slab thickness was defined as $h/a=0.52$. The FDTD calculated spectrum is in good agreement with the experimental transmission spectrum. The difference in amplitude is due to the shorter waveguide length used in the calculations (33 unit cells or 14.4 μm). The comparison of calculated and experimental transmission spectra allows identification of the measured transmission cutoff around 1700 nm as the onset of the waveguiding mode. The onset is followed by numerous resonances starting at 1725 nm. In direct analogy with the interpretation of the experimental results shown in Figs. 1(b) and 3(a), these resonances can be attributed to modes below the LBE.

The calculation also confirms the presence of additional resonances between 1200 and 1500 nm. However, from the FDTD spectrum alone it is not possible to assign their origin. To address this issue Fig. 4(b) presents photonic band structure calculation with identical structural input parameters as for Fig. 4(a). The strong resonances clearly match with slab modes whose spectral onset defines the UBE. The UBE, not visible in the previous spectra of Figs. 1(b) and 3(a), has now redshifted over 400 nm and almost spectrally matches the position of the light line cutoff. This huge spectral shift of the UBE is far more pronounced than the shift of the LBE. As mentioned before, UBE (air) modes are mainly located in the holes of the PhC and thus exhibit a strong dependence on hole radius. In the experimental transmission spectrum of Fig. 4(a), a kink around 1570 nm indicates where the waveguiding mode crosses the light line. This becomes more visible for longer waveguide lengths as shown in Fig. 3(b) (note this is for $r/a\sim0.23$). The bandwidth for LLP in Fig. 4(a) is now close to 130 nm, an increase of nearly 300%. This very broad bandwidth is confirmed by comparison with the corresponding photonic band structure in Fig. 4(b).

Losses within the LLP band are determined from transmission spectra of PhC waveguides with different lengths. The inset in Fig. 4(a) shows the measured transmission loss at 1650 nm with the waveguides normalized with respect to a single-mode reference strip waveguide.

The obtained slope of the transmission attenuation yields 3 ± 2 dB/cm. Note that this number does not correspond to the propagation losses of the PhC waveguide itself but rather to the losses of the whole photonic circuit (PhC waveguide and access strip waveguides). With increasing length of the PhC waveguides (increasing losses) the length of the strip waveguides is shortened (decreasing losses) to keep the total length of the photonic circuit on a chip constant at 4.6 mm. The obtained slope therefore underestimates propagation losses of the PhC waveguide. As it was pointed out in Ref. 10, for a correct determination the losses in the bare strip waveguide have to be taken into account. The transmission of analogous strip waveguides with a 460×220 nm^2 cross section have been measured as a function of the length (4.7–21 mm). Losses were determined as 3.6 and 5 dB/cm at 1500 and 1650 nm, respectively, as reported elsewhere.[21] Correspondingly, the effective loss of the PhC waveguide at 1650 nm can be estimated as 8 ± 2 dB/cm. To our knowledge, this is one of the lowest loss numbers reported for SOI PhC waveguides. There is a remarkable dependence on the hole radius with losses decreasing from 24 ± 3 dB/cm for $r/a=0.365$ (Ref. 10) to 20 ± 3 dB/cm for $r/a=0.34$ and to 8 ± 2 dB/cm for $r/a=0.23$. It can be argued that the surface area of the holes is significantly decreased in the waveguides with smaller radii; thus, scattering losses due to sidewall roughness are becoming less pronounced. In addition, the effective waveguide width increases with decreasing hole radius which can further reduce losses.

Figure 5 summarizes the experimental results of the PhC waveguides for all measured hole radii. The spectral positions of the TE spectra such as stop band, UBE, LBE, light

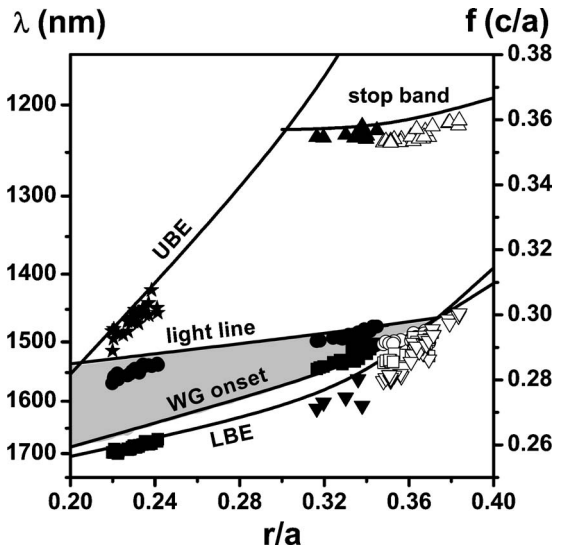

FIG. 5. Experimentally derived TE map depicting spectral positions of stop band (triangles up), UBE (asterisks), light line (circles), WG onset (squares), and LBE (triangles down) as a function of the hole radius $r/a=0.22-0.38$. Solid lines represent 3D plane-wave band structure calculations with input parameters determined from SEM measurements for hole radii with $r/a=0.32-0.34$.

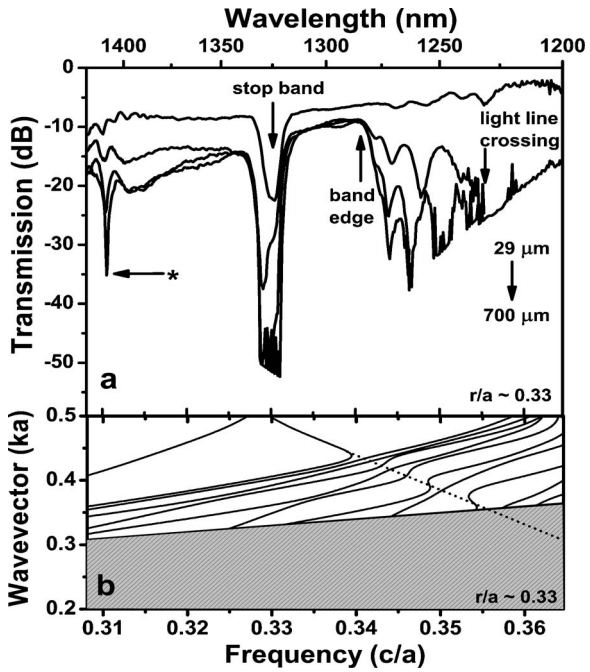

FIG. 6. (a) Length series of TM transmission spectra of PhC waveguides (29–700 μm) with hole radii $r/a\sim0.33$. The transmission dip marked with an asterisk corresponds to the x-odd TE-like mode (see text for details). (b) 3D plane-wave band structure calculations. The dotted line indicates the fundamental TM-like waveguiding mode.

line, and waveguiding onset are shown as a function of the normalized hole radius (open shapes correspond to data from Fig. 2). The experimental results are compared to 3D plane-wave calculations (solid line) for the slab thickness h taken as $0.473a$. This corresponds to the hole size series ranging from $r/a=0.32$ to 0.34. Good agreement between experiment and calculation is found. The results in Fig. 5 demonstrate that with decreasing hole radii the broadening of the bandwidth for low-loss propagation is accompanied by a simultaneous shrinkage of the PBG. Between the three different size series a spectral displacement with respect to each other can be seen. This steplike behavior is due to the different slab thicknesses h of the SOI wafers as measured with a SEM (see Sec. II).

The plane-wave calculations in Fig. 5 indicate that for hole radii of $r/a=0.207$ a maximum LLP with over 150 nm bandwidth is achievable. While PBG bandwidth is reduced to 160 nm, the LLP region covers already 94% of it. A further decrease of the hole radius would appear to reduce the LLP bandwidth as the slab modes of the UBE would merge into the LLP.

V. TRANSMISSION OF THE TM-LIKE MODES IN PHC WAVEGUIDES

It is well known that a PBG for the TM-like modes does not exist for SOI PhC slabs.[15] However, it is important to characterize the transmission characteristics of PhC waveguides for the TM mode as well. First, measurements of TE- and TM-like modes provide good verification and validation of the theoretical fitting. With a set of only three fitting parameters (hole radius, refractive index, and slab thickness) all spectral features found in both TE and TM spectra have to simultaneously match the band structure calculations. Second, and more importantly, due to possible imperfections and errors in the experimental structures, TM-like modes in principle may interact with the TE-like modes of interest and cause additional propagation losses.[11]

Measured transmission spectra of TM-like modes are shown in Fig. 6(a). The hole radius of the PhC waveguides is $r/a\sim0.33$. The length of the different photonic crystals ranges from 29 to 700 μm. All transmission spectra exhibit a strong dip at around 1325 nm, as well as multiple strong resonances starting at 1280 nm and extending up to the transmission cutoff at 1235 nm. As before, 3D plane-wave calculations of the photonic band structure are helpful in interpretation of the spectral features [Fig. 6(b)]. A dotted line indicates the fundamental TM-like waveguiding mode. Both in- and out-of-plane confinements of the mode are purely index guided, hence showing a nearly linear dispersion. However, the mode is still strongly confined in the PhC waveguide and provides most of the transmission. The dip at 1325 nm can be identified as a stop band that arises from the folding of the fundamental mode at the edge of the Brillouin zone. This fundamental mode is crossing the light line at around $0.355/a$, which explains the appearance of the cutoff at 1235 nm. Multiple resonances between 1280 and 1235 nm are arising from the coupling of the fundamental mode with numerous slab modes. Such behavior is very analogous to the mode mixing mechanism observed recently in SOI double-trench waveguides.[11] The spectral region between the stop band at 1325 nm and the onset of the resonances at 1280 nm are characterized by relatively low-loss propaga-

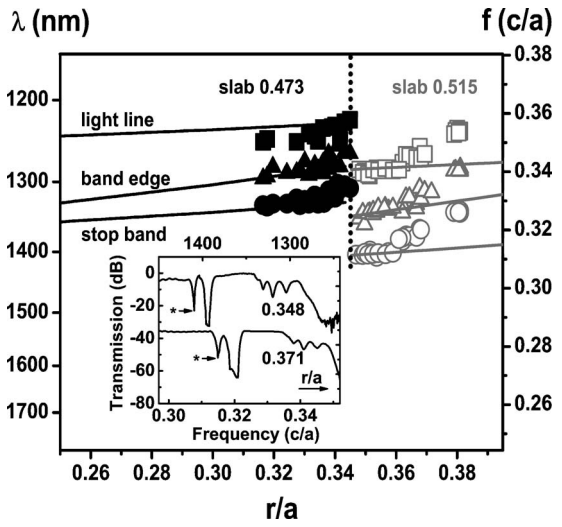

FIG. 7. Experimental TM map of the spectral positions of light line (squares), band edge (triangles), and stop band (circles) as a function of the hole radius $r/a=0.32-0.38$. Solid lines represent 3D plane-wave band structure calculations (black and grey) with input parameters according to the experimental SEM results for hole radii of $r/a=0.32-0.34$ and $r/a=0.35-0.38$, respectively. Inset: TM spectra of two PhC waveguides, identical in length (29 μm), but with different hole radii ($0.348a$ and $0.371a$). The transmission dips marked with an asterisk correspond to the x-odd TE-like mode (see text for details).

tion. Measurements at 1300 nm indicate losses as small as 16 ± 3 dB/cm.

The results of the analyzed TM transmission spectra for hole radii from $r/a=0.32$ to 0.38 are summarized in Fig. 7. The solid lines are derived from photonic band structure calculations. For the two size series, a slab thickness of $h/a=0.473$ or 0.515 was chosen as an input parameter. These are the same values as for the corresponding TE-like photonic band structures in Figs. 6 and 1, respectively. The calculations are in good agreement with the experimental results. The inset of Fig. 7 shows the TM spectra of two waveguides, identical in length (29 μm), but different hole radii ($0.348a$ and $0.371a$). The shift of the transmission spectra for differently chosen hole radii is clearly visible. However, comparison with the corresponding TE spectra of the identical waveguides [see Fig. 1(b)] shows that the TM modes exhibit a less pronounced dependence on the hole radius. In contrast to this, comparing the map of TM-like modes in Fig. 7 to the map of TE-like modes in Fig. 5, the spectral shift between the series of different SOI wafers is far more pronounced. Such behavior is not unexpected since TM-like modes are polarized perpendicular to the slab plane and are therefore strongly influenced by a change in the slab thickness and less by the hole radius.

VI. COUPLING BETWEEN EVEN AND ODD MODES

In principle, a W1 SOI waveguide is not single moded over the entire bandwidth of the PBG. It is known that it can support two TE-like modes (both even with respect to the xy plane in the slab) possessing different symmetries with respect to the zx plane which vertically bisects the slab along the waveguide direction (x axis). All results presented so far correspond to the in-plane x-even TE-like mode. This mode is of most interest for integrated photonics.[4–14] The TE-like mode with odd zx symmetry is visible in all band structure calculations [e.g., Fig. 1(a) at $c/a=0.31$]. However, the excitation of this x-odd TE-like mode with the x-even TE mode in the access strip waveguide is prohibited due to symmetry restrictions. The orthogonality of the x-even and x-odd TE-like modes in the PhC waveguides also prohibits any interaction. Correspondingly, the odd mode is usually not observed in transmission spectra and its properties are regarded as irrelevant to waveguiding in PhC waveguides.

Indeed, in the experimental TE spectra of PhC waveguides with large hole radii [Fig. 1(b)] no evidence of this mode at 1430 nm ($r/a=0.348$) or 1390 nm ($r/a=0.379$) is observed. TE transmission spectra of PhC waveguides with small hole radii [Fig. 3(b)] are also well explained by the photonic band structure and FDTD calculations, as discussed above. However, there is another spectral feature present in these spectra, which does not fit into this picture of forbidden mode coupling. At wavelengths around 1600 nm, a distinct breakdown within the LLP region is observed [marked with an asterisk in Fig. 3(b)]. Its strength gradually increases as a function of the PhC waveguide length. As seen from the band structure calculations in Fig. 4(b), no other modes except the in-plane x-odd TE-like mode are present in this spectral range. Since no indication of the x-odd TE-like mode is visible in the spectra of short waveguides [Figs. 1(b) and 3(b)], we can conclude that this is not an interface phenomenon but rather the x-even TE-like mode, being excited from the strip waveguide and gradually transferring energy to the x-odd mode. The field energy, once transferred, cannot couple efficiently into the output strip waveguide due to symmetry restrictions and therefore dissipates in the slab. Correspondingly, the x-even TE-like mode exhibits additional propagation losses, which can be estimated from Fig. 3(b) as 20 dB/cm at the center of the dip around 1600 nm. This weak mode coupling explains the absence of the x-odd mode in Fig. 1(b) since the presented PhC waveguides are only 29 μm in length and the resulting losses would only be $\sim$0.5 dB. Furthermore, the frequency range where both modes coexist is located far above the light line [$c/a\sim0.32$ in Fig. 1(c)] where diffraction losses due to out-of-plane leakage dominate.

In general, the presence of both modes in the experimental spectra indicates that the perfect symmetry of the PhC lattice with respect to zx plane is somehow relaxed and the interaction between the modes can become possible. In principle two different mechanisms can be considered that might cause the violation of symmetry in the otherwise highly symmetric (001) plane of the SOI wafer: structural irregularities in the PhC lattice or in-plane optical anisotropy.

Asymmetry in the waveguide can in principle be introduced by structural imperfections of the PhC lattice. Sidewall surface roughness was measured to be only a few nm (Ref. 21) and therefore is believed to be an unlikely candidate. Small lateral offsets of the crystal can occur due to imperfect field and subfield stitching when devices are de-

fined with electron-beam lithography. Offsets in the y axis would result in an xz asymmetry of the PhC waveguide and could be a possible cause of mode mixing. A field (with dimensions of 400 μm) usually has a stitch error $<10-20$ nm while subfields (~ 6 μm) are typically even smaller; however, the impact of stitching error requires further systematic investigation. A further possible source of asymmetry is stress in the Si film. While Si is a cubic crystal and should therefore be optically isotropic, small birefringence ($\Delta n \sim 10^{-6}$) has been reported.[22] Significant birefringence can be induced by stress and is a known problem for SOI rib waveguides.[23] However, for released Si membranes fabricated on Unibond SOI wafers[24] it is difficult to expect strain higher than a few tens of MPa. Further investigation is necessary to confirm the origin of the observed mode mixing.

Interestingly, the spectral signature of the x-odd TE-like mode can also be identified in TM transmission spectra. For example, the data in Fig. 6(a), which shows TM transmission spectra of PhC waveguides with $r/a=0.33$, exhibit a pronounced dip around 1410 nm (again marked with an asterisk). Similar dips are also observed in the TM transmission spectra of PhC waveguides of larger hole radii (inset of Fig. 7). The corresponding photonic band structure of the TM modes in Fig. 6(b) cannot explain this spectral feature. Instead, its spectral position exactly coincides with the x-odd TE-like mode at the edge of the Brillouin zone at $k=0.5$ [Figs. 1(a), 1(c), and 4(b)].

The spectral positions of these dips in both TE and TM spectra are plotted in Fig. 8. Data points for $r/a=0.22-0.24$ are taken from TE spectra and for $r/a=0.32-0.38$ from TM spectra. The solid line represents the calculated dependence of the x-odd TE-like waveguiding mode on the hole radius for a slab thickness of $h/a=0.473$. In analogy to Fig. 5, the spectral steplike shift between the different size series again follows the change in the slab thickness. Remarkably all data points for both TE and TM spectra are in good agreement with plane-wave calculations for the x-odd TE-like mode over the entire range of hole radii.

Just as for the TE-like transmission spectra, the attenuation of the dip in the TM spectra gradually increases with the waveguide length. We can therefore again exclude any significant contribution of energy transfer between the modes at the interface between the strip waveguide and the PhC. The energy transfer between the TM-like and TE-like x-odd modes is taking place gradually while the light is propagating along the waveguide.

VII. SUMMARY

In this paper we have performed an extensive investigation of the transmission properties of SOI-type PhC W1 waveguides as a function of the hole radius, slab thickness, and crystal length for both TE and TM polarizations. Our experimental results reveal that for structural parameters optimized for maximization of the PBG, the bandwidth for low-loss propagation below the light line cutoff completely vanishes for hole radii $r/a>0.37$. This is mainly caused by a tremendous spectral shift of the lower band edge slab modes, which are mostly localized in the slab surrounding the holes and are strongly influenced by a decrease of the average refractive index of the slab. PhC W1 waveguides with a maximized PBG are therefore unsuitable for integrated photonics applications. The experimental findings for PhC waveguides possessing small holes with only $r/a \sim 0.2$ demonstrate that the bandwidth for transmission can be maximized to almost 130 nm while still maintaining a sufficient PBG. Losses for these devices are reduced to only 8 dB/cm presumably due to the significantly smaller surface area of the etched holes. The experimental transmission spectra for both TE and TM polarizations show very good agreement with calculated photonic band structures and 3D FDTD transmission spectra.

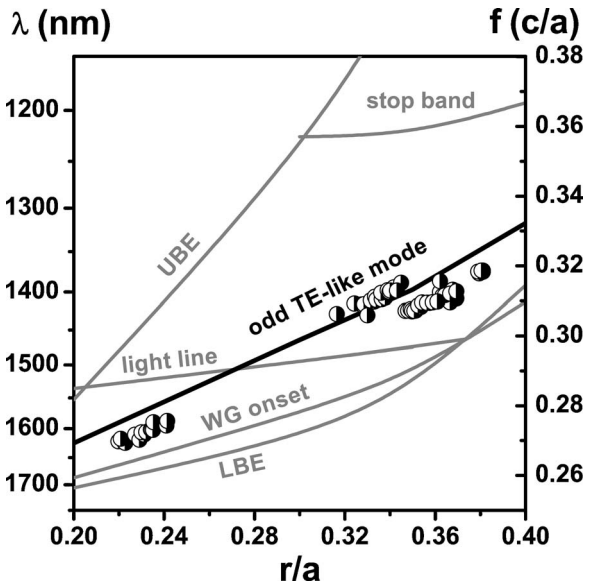

FIG. 8. Experimental map of the x-odd TE-like waveguiding mode as a function of the hole radius. Solid lines represent 3D plane-wave band structure calculations with input parameters according to SEM measurements for hole radii of $r/a=0.32-0.34$. The black line plots the x-odd TE mode while the grey lines represent the UBE, light line, WG onset (even TE mode), stop band, and LBE from Fig. 5.

ACKNOWLEDGMENTS

The authors gratefully acknowledge useful discussions with N. Moll (IBM Zurich Research Lab) and G.L. Bona (IBM Almaden Research Lab) and the contributions of the Microelectronics Research Laboratory staff at the IBM T. J. Watson Research Center.

*Corresponding author. Electronic address: fdulkei@us.ibm.com

[1] T. F. Krauss, R. M. De La Rue, and S. Brand, Nature (London) **383**, 699 (1996).
[2] T. Baba, N. Fukaya, and J. Yonekura, Electron. Lett. **35**, 654 (1999).
[3] S. Y. Lin, E. Chow, S. G. Johnson, and J. D. Joannopoulos, Opt. Lett. **25**, 1299 (2000).
[4] T. Baba, N. Fukaya, and A. Motegi, Electron. Lett. **37**, 761 (2001).
[5] M. Loncar, D. Nedeljkovic, T. Doll, J. Vuckovic, A. Scherer, and T. P. Pearsall, Appl. Phys. Lett. **77**, 1937 (2000).
[6] M. Loncar, T. Doll, J. Vuckovic, and A. Scherer, J. Lightwave Technol. **18**, 1402 (2000); M. Loncar, D. Nedeljkovic, T. P. Pearsall, J. Vuckovic, A. Scherer, S. Kuchinsky, and D. Allan, Appl. Phys. Lett. **80**, 1689 (2002).
[7] M. Notomi, A. Shinya, K. Yamada, J. Takahashi, and I. Yokohama, Electron. Lett. **37**, 293 (2001).
[8] M. Notomi, K. Yamada, A. Shinya, J. Takahashi, C. Takahashi, and I. Yokohama, Phys. Rev. Lett. **87**, 253902 (2001).
[9] W. Bogaerts, V. Wiaux, D. Taillaert, S. Beckx, B. Luyssaert, P. Bienstman, and R. Baets, IEEE J. Sel. Top. Quantum Electron. **8**, 928 (2002).
[10] S. J. McNab, N. Moll, and Yu. A. Vlasov, Opt. Express **11**, 2927 (2003).
[11] Yu. A. Vlasov, N. Moll, and S. J. McNab, J. Appl. Phys. **95**, 4538 (2004).
[12] M. Zelsmann, E. Picard, T. Charvolin, E. Hadji, M. Heitzmann, B. Dalzotto, M. E. Nier, C. Seassal, P. Rojo-Romeo, and X. Letartre, J. Appl. Phys. **95**, 1606 (2004).
[13] Y. Sugimoto, Y. Tanaka, N. Ikeda, Y. Nakamura, K. Asakawa, and K. Inoue, Opt. Express **12**, 1090 (2004).
[14] M. Notomi, A. Shinya, S. Mitsugi, E. Kuramochi, and H.-Y. Ryu, Opt. Express **12**, 1551 (2004).
[15] S. G. Johnson, S. Fan, P. R. Villeneuve, J. D. Joannopoulos, and L. A. Kolodziejski, Phys. Rev. B **60**, 5751 (1999).
[16] S. G. Johnson, P. R. Villeneuve, S. Fan, and J. D. Joannopoulos, Phys. Rev. B **62**, 8212 (2000).
[17] A. Chutinan and S. Noda, Phys. Rev. B **62**, 4488 (2000).
[18] E. Chow, S. Y. Lin, S. G. Johnson, P. R. Villeneuve, J. D. Joannopoulos, J. R. Wendt, G. A. Vawter, W. Zubrzycki, H. Hou, and A. Alleman, Nature (London) **407**, 983 (2000).
[19] S. G. Johnson and J. D. Joannopoulos, Opt. Express **8**, 173 (2001).
[20] Rsoft Design Group, FULLWAVE 4.0 Manual, 2005.
[21] Yu. A. Vlasov and S. J. McNab, Opt. Express **12**, 1622 (2004).
[22] J. Pastrnak and K. Vedam, Phys. Rev. B **3**, 2567 (1971).
[23] See, for example, D.-X. Xu *et al.*, Opt. Lett. **29**, 2384 (2004).
[24] G. K. Celler and S. Cristoloveanu, J. Appl. Phys. **93**, 4955 (2003).